Research paper

Mechanical behavior improving study of concrete deck of main beam at pylon root of composite beam cable-stayed bridge

Tianyu Qi[1], Chao Wang[2], Xiang Pan[3], Guining Han[4]

Abstract: Steel-concrete composite beam has been increasingly applied to large span cable-stayed bridges. It takes full advantage of the material properties of steel and concrete. However, the concrete deck bears tension in the negative moment zone, such as zero block, which is disadvantageous to structures. Aiming at this problem, a finite element model of the zero block in the negative moment zone of a semi-floating cable-stayed bridge is built, and the local mechanical performance of the bridge deck under completed status is studied. Based on the analysis results, three improvement measures have been proposed. The improvement effect of each method and composed of three methods has been studied. The numerical results show that the whole zero block zone is in the compressed state under the combined action of the bending moment and axial force of the stay cable. However, the local negative moment effect in the zero block zone is very prominent under the support of the diaphragm plate. Removing parts of the diaphragm plate at the bearing position can significantly improve local mechanical behavior in the concrete deck, which transfers the local support to the adjacent two diaphragm plates. The composed improvement effect is prominent when the three measures are adopted simultaneously.

Keywords: steel-concrete composite structure, negative bending moment zone, bridge deck, finite element analysis, zeroblock

[1]M.Sc., Eng., Hubei University of Technology, School of Civil Engineering, Architecture and Environment, Wuhan. Hubei, China, e-mail: qitianyu0523@163.com, ORCID: 0009-0005-6278-751X
[2]Prof., Eng., Hubei University of Technology, School of Civil Engineering, Architecture and Environment, Key Laboratory of Intelligent Health Perception and Ecological Restoration of Rivers and Lakes, Ministry of Education, Wuhan. Hubei, China, e-mail: wangc800@126.com, ORCID: 0000-0002-5984-0851
[3]M.Sc., Eng., Hubei University of Technology, School of Civil Engineering, Architecture and Environment, Wuhan. Hubei, China, e-mail: px000306@163.com, ORCID: 0009-0009-7760-5589
[4]M.Sc., Eng., Hubei University of Technology, School of Civil Engineering, Architecture and Environment, Wuhan. Hubei, China, e-mail: hugnhan@126.com, ORCID: 0009-0002-7942-6989

1. Introduction

A steel-concrete composite beam bridge is composed of steel beams and concrete bridge deck, which are combined by shear connectors. This kind of structure makes full use of the tensile properties of steel and the compressive performance of concrete, and it is more suitable for large-span bridge structures because it has many advantages such as high stiffness, short construction period, and good economic benefits [1, 2]. However, in the negative bending moment zone, the concrete bridge deck is subjected to tensile stress, and the steel beam is subjected to compressive stress, which is an unfavorable stress state for the steel-concrete composite beam structure. When the tensile stress exceeds the strength of the concrete, the cracks appear and decrease the whole stiffness of the composite structure, leading to further deterioration of the stress state. Meanwhile, the compression of the steel beam will easily lead to local buckling, which limits the development of the steel-concrete composite beam bridge [3, 4]. To make this type of structure widely used and obtain better economic benefits, it is necessary to overcome this stress defect in the negative bending moment zone. Many scholars have carried out much research work on this problem [5–7]. Song et al. [8] adopted the numerical analysis method to study the improvement in the inelastic mechanical property of steel-concrete composite beams under a negative moment, which was strengthened by carbon-fiber-reinforced polymer laminates. Sun et al. [9] proposed a three-dimensional reinforcement design method for pre-stressed concrete box-girder bridges with a specific spatial lattice grid model, and they [10] further proposed the single-layer folding surface grillage and spatial grillage method for the practical and precise modeling of concrete box-girder bridges. Zhu et al. [11] carried out an experimental test to investigate the flexural behavior of steel-UHPC composite beams with waffle slabs in negative moment regions. They developed theoretical models to calculate the ultimate flexural capacity of steel-UHPC composite beams with waffle slabs under negative moments. Liu et al. [12] studied the performance improving method of bridge deck in the negative moment zone of a steel-concrete composite beam bridge. Three measures are usually taken to decrease the stress level in concrete slabs in the negative bending moment zone, so it can prevent and control the development of cracks. The first method is adopting a new structure style [13–15]. The second measure is applying pre-stress in concrete slab [16–19]. However, the construction is complicated on site. Replacing ordinary concrete with other high-performance concrete, which has higher tensile strength, is another effective method [20–23].

For the semi-floating cable-stayed bridge, the main beam is usually constructed by cantilevering. The first segment at the tower location is built on a bracket, and the other segments are cantilever symmetrical constructed. As shown in Fig. 1, the first section at the tower location is named Zero(0#) Block in this paper, and the other segments are called in turn 1# block, 2#block.

Due to the constraint of the bearing, there is a negative moment peak at zero block, which induces a very large local stress concentration. When a steel-concrete composite beam is adopted in this type of bridge, the stress state of the concrete bridge deck at zero block is very complex, so it is crucial to do in-depth research. In this paper, a finite element
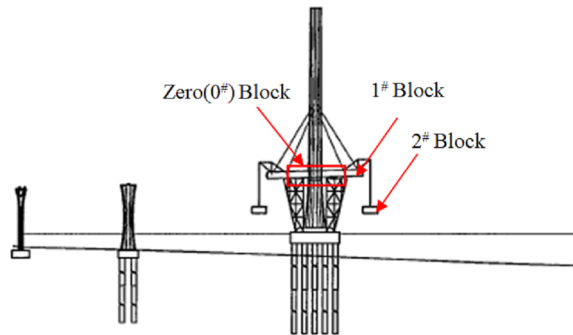
Fig. 1. Segments installation schematic of main beam cantilever construction

model of the zero block in the negative moment zone of a semi-floating cable-stayed bridge is built, and the local mechanical performance of the concrete bridge deck under completed status is studied. Based on the research results, three improvement measures have been proposed, and the improvement effects of the methods have been researched.

2. Bridge description

The analyzed practical engineering here is a semi-floating steel-concrete composite beam cable-stayed bridge with a single cable plane and twin towers. And the cross-section of the composite beam is designed as a single box with three cells. The main span is 360 m, and the side span is 160 m of the bridge. Due to the different mechanical behavior along the longitudinal bridge, the steel beam is composed of multi-type segments. For the standard segments applied in mid-span, the roof of the steel box beam is open, and a diaphragm plate is set every 4 m. However, for the segments near the cable pylon, the roof is closed. At the connection section of the open and closed roof, two diaphragm plates are installed at 1.5 m intervals, and then 2 m intervals of diaphragm plates are kept to the center position of the cable pylon. Pre-stressed tendons have been arranged in the concrete bridge deck alone longitudinal and transverse directions. The steel strands with $9\varphi^s$ 15.2 mm and $12\varphi^s$ 15.2 mm are used in the concrete bridge deck near the cable pylon. Pre-stressed fine-rolling screw-thread steel bars are adopted for cantilever assembly of main beam segments, and the steel strand with the type of $4\varphi^s$ 15.2 mm is used to apply transverse pre-stressed in the concrete bridge deck. Because a single-column cable pylon is designed, a hole with 12×5.4 m is reserved in the main beam at the position of zero block, so the cable tower directly passes through the main beam. Two bearings are symmetrically arranged at the bottom of the main beam in zero block with a distance of 7.65 m. The cables are arranged at 8m from the main beam, and the cable distance on the tower is 2.5 m. The cross-sectional layout of the main beam is shown in Fig. 2. Because the bridge is still under construction, a rendering is presented in Fig. 3.
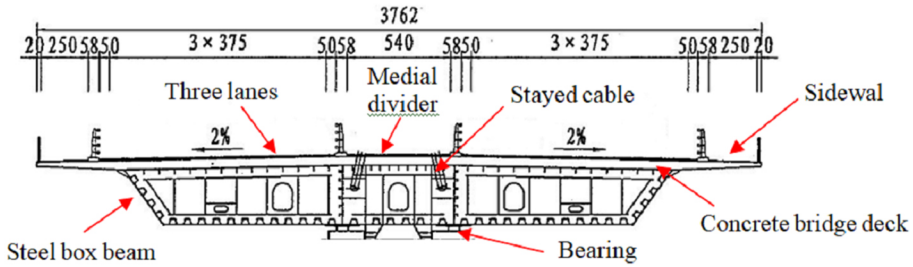
Fig. 2. The cross-sectional layout of the main beam
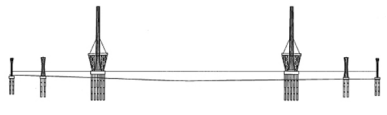

Fig. 3. The rendering of the practical bridge
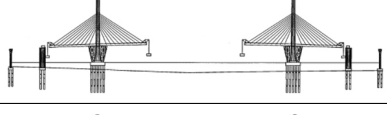
3. Global numerical analysis

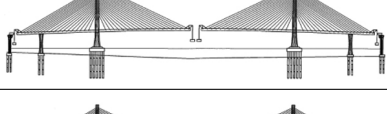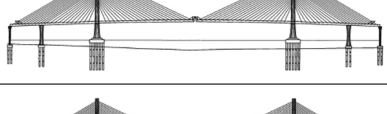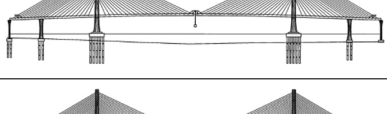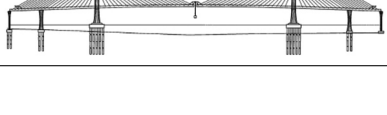For details studying the mechanical performance of zero block in the negative moment zone of the bridge, a complex local finite element model needs to be built. Considering the boundary conditions have a large influence on the mechanical behavior of the truncation local model, a global analysis of the full-bridge model has been conducted first, and then the internal force of the main beam at the root section of the pylon was extracted. The global analysis results would be used to determine the boundary conditions of the local model, which could make it more accurate to simulate the practical force status.

Firstly, we build the full-bridge finite element model. Because the internal force status of a cable-stayed bridge is closely related to its construction process, it is necessary to simulate the construction process of the whole bridge in detail. The major structure of the bridge is constructed according to the following seven steps listed in Table 1.

The steel-concrete composite beam was simulated by a single beam, and the composite section was adopted, in which the section of the concrete deck was equated with the steel structure according to the plane section assumption. After equivalence processing, the neutral axle of the equivalent section kept consistent with that of the original section, and the section area of concrete was reduced according to the elasticity modulus ratio of concrete and steel, so the stress of concrete deck could be deduced based on the strain of the equivalent steel structure. The density of the main girder element was calculated based on the equivalent section area to ensure that the total mass was equivalent to that of the original composite

Table 1. Internal force and stress of the primary beam in the section of tower root

Step 1		Finish the construction of pylons, transition piers, auxiliary piers, and zero blocks, and stretch the longitudinal and transverse pre-stressed tendons, and then stretch the cable of No.1
Step 2		Build the segments of main beam from No.2 to the secondary side span by double cantilever construction, and then stretch corresponding pre-stressed tendons and cable.
Step 3		Construction and closure segments of the secondary side span and corresponding pre-stressed
Step 4		Construction of side span and closure segment
Step 5		Build the segments of the main span by single cantilever construction, and then stretch the corresponding pre-stressed tendons and cable
Step 6		Construct the closure segment of the midspan, and then release the temporary constraint between the pylon and the main beam
Step 7		Adjust the cable force of the full bridge and construct the bridge deck system

beam, including all local reinforcement. The towers and piers were all simulated using beam elements. The cables were simulated by truss elements. Considering that the center of the main girder was not in line with the endpoint of the tension cables, multiple rigid arms were used to connect the cables and the main girder, which had great stiffness but no mass. Figure 4 showed the localized zoomed-in connection configuration circled with a red ellipse. The whole bridge model was simulated with 1211 nodes and 1270 elements. Fixed constraints were set at the bottom of all piers. The main girders were set fixed constraints at the top of all piers along the vertical bridge, and elastic constraints with stiffness of 10^8 kN/m were set along the transverse and longitudinal bridge. The weight of the bridge and secondary dead load, such as pavement layer, railings, etc, which is 137 kN/m, were applied in global analysis. The global finite element model of the whole bridge was shown in Fig. 4.
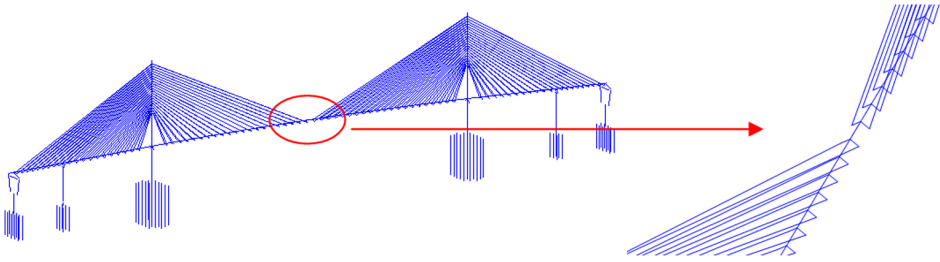
Fig. 4. The global finite element model of the whole bridge

By simulating the whole construction process until the completion state using finite element analysis, we could extract the internal force and stress of the structure in the finished bridge state. Because the force status of the main beam was focused here, for the convenience of display, only the analysis results of the half-span bridge were extracted, and the cable tower was removed. The vertical bending moment, axial force, vertical shearing force, and upper edge stress of the concrete deck were shown in Fig. 5 as follows. The unit of moment, force, and stress was kN·m, kN, and kPa, respectively.

The calculated internal force and stress results of the main beam at the root center section of the pylon, which was also the center of the zero block, were shown in Table 2 below.

Table 2. Internal force and stress results of the main beam at the root section of the pylon

Axial force (kN)	Shear force $-y$ (kN)	Shear force $-z$ (kN)	Bending moment $-y$ (kN·m)	Bending moment $-z$ (kN·m)	Upper edge stress (kPa)
−197193.0	0.04	7798.26	−138538.0	7.7	−3395.3

Note: The $-y$ denotes the transverse direction, and the $-z$ denotes the vertical direction.

As shown in Fig. 5, there is a significant negative bending moment segment of the main beam near the root of the pylon under the complete bridge state (circled by the red line), which is due to the vertical constraint of the bearing. However, unlike the general continuous beam structure, the bridge is a composite beam cable-stayed bridge, in which structure there is a large axial pressure in the main beam at the root of the pylon, the negative bending moment section. Under the combined action of the bending moment and axial force, there is no tensile stress on the upper edge of the main beam in the zero block segment, and there is some compressive stress reserve under the completed status. However, because the pylon passes through the main beam at zero block segment, there is hollow and section mutation in the main beam, and the local stress status is very complex. It is necessary to build a local finite element model of zero block for a more detailed simulation analysis.
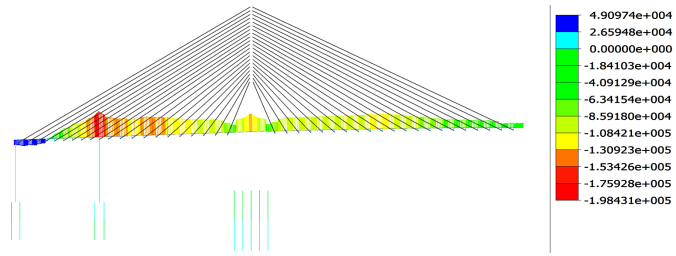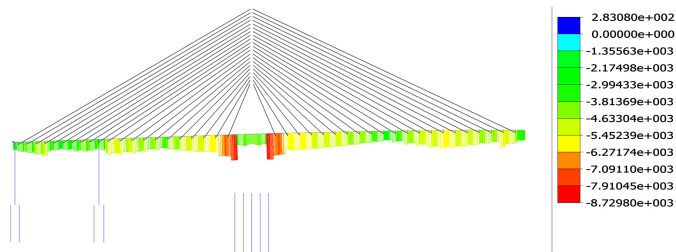
(a)
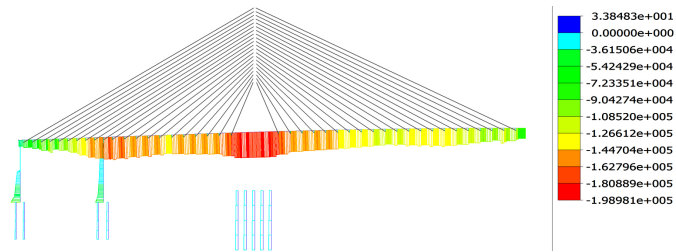
(b)
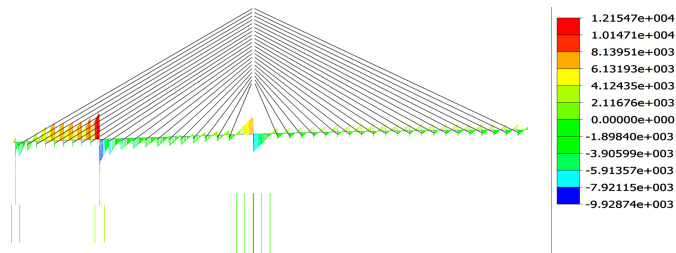
(c)

(d)

Fig. 5. The global analysis results of the main beam under the completion bridge state
(a) vertical moment, (b) axial force, (c) vertical shearing force, (d) upper edge stress

4. Local numerical analysis

Here, two 10-meter steel-concrete composite beam segments along the longitudinal bridge from the pylon to the mid-span and side-span were truncated to build a local model of zero block. The cross-section of the composite beam at the root of the pylon was shown in Fig. 6.
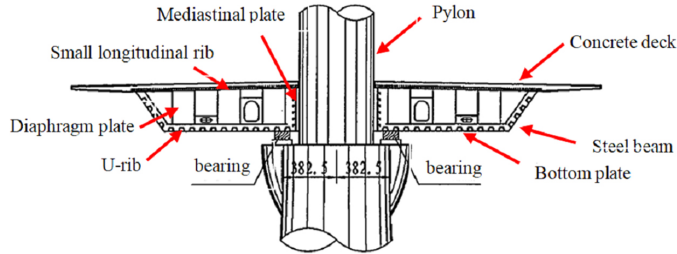

Fig. 6. The cross-section of the composite beam at the root of the pylon

For the convenience of calculation, half of the structure along the transverse bridge was used to build the finite element model based on symmetry. The general commercial FEM software ANSYS was adapted to simulate the local model of zero block. Steel structure parts, including the top plate, bottom plate, diaphragm plate, mediastinal plate, small longitudinal rib, stiffening plate, etc., were simulated by the shell element (Shell63). The pre-stressed bars were simulated as bar elements (Link8), and the concrete bridge decks were built with solid elements (Solid45). Because the bolt connection between the concrete deck and the steel box girder was not the focus of this paper, they were set as fully connected. The meshing sizes of main focus parts were refined to 25 cm, including the concrete bridge deck, diaphragm plate, and pre-stressed bars. The other parts of the structure, including the bottom plate, mediastinal plate, small longitudinal rib, and U rib, were meshed with a size of 40 cm. The material elastic modulus of steel and concrete structure was set as 2.06×10^{11} Pa and 3.6×10^{10} Pa, and the Poisson ratio was set as 0.3 and 0.2, respectively. The whole model was simulated with 80703 elements and 88929 nodes. For the convenience of applying boundary conditions, both ends of the local solid model were assembled with rigid arm elements. The detailed local finite element model was shown in Fig. 7a. For clearly showing the internal structure, part of the concrete deck was removed, as shown in Fig. 7b.

During the global analysis, the construction process of the bridge, the shrinkage, and the creep of concrete were all simulated in detail. However, only the final state was analyzed in the local model, which didn't simulate the practical construction process, so it was difficult to ensure that the internal force calculated by the local model was entirely consistent with the result of global analysis. Here, we mainly focused on the stress status of the disadvantage section of zero block in the negative moment zone, which was the root section of the pylon marked with a red dotted line box in Fig. 7b. To ensure the internal force result at the root section of the pylon calculated by local analysis, including the bending moment, axial force, and shearing force, was consistent with that of the global analysis result listed in Table 2,
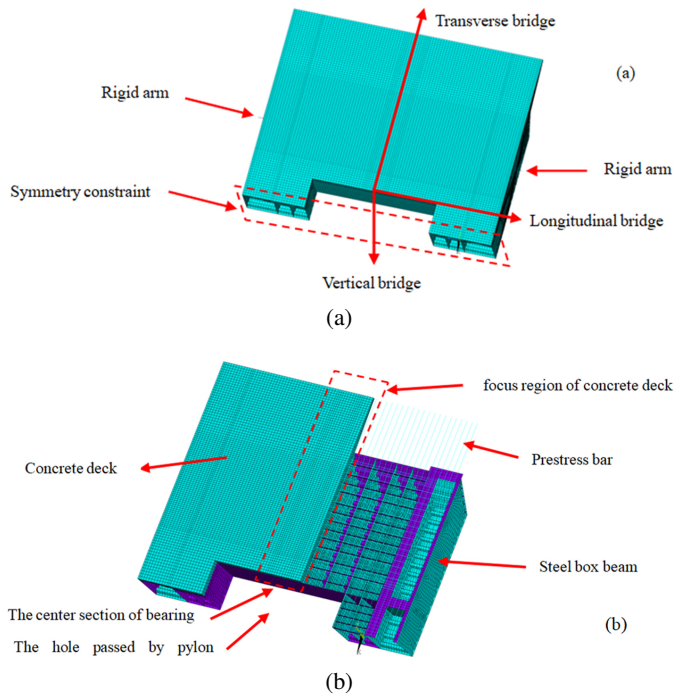
Fig. 7. Detailed view of the local finite element model of zero block (a); Internal structure of the local model (b)

we need to apply appropriate boundary conditions at both ends of the local model. It was calculated by building a local beam model shown in Fig. 8.
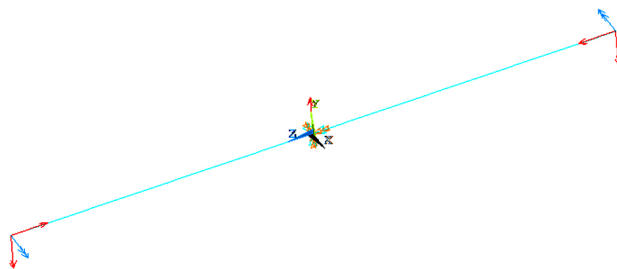

Fig. 8. The local beam model of zero block for calculating boundary conditions

By optimizing the load applied on both ends of beam model, we could make the internal force of the root section of the pylon agree with the result listed in Table 2. The optimized external loads were listed in Table 3.

The optimized external loads were applied on both ends of the rigid arm in the local solid model, as shown in Fig. 7a. The section of bearing shown in Fig. 6 and Fig. 7a was applied

Table 3. The optimized external load applied on both ends of beam model

Vertical force (kN)		Axial force (kN)		Bending moment (kN·m)	
Left end	Right end	Left end	Right end	Left end	Right end
–442.5	–442.5	–69981.8	70207.5	67561.5	–67322.5

vertical constraint. Because only half of the local model of zero block along the transverse bridge was simulated, the symmetric constraints were applied on the symmetry section, which was marked with a red dotted line box in Fig. 7a. The bridge's weight and secondary dead load including pavement layer, railings, etc, which is 137 kN/m, were calculated in local analysis.

As mentioned above, we mainly focused on the stress status of the concrete deck of the root section of the pylon, which was marked with a red dotted line box in Fig. 7b. Through finite element analysis of the local solid model, we can obtain the stress status of the focused concrete deck. For a more precise display of the stress status, only the results of the focused concrete deck were extracted and analyzed. The longitudinal stress results were shown in Fig. 9. The direction coordinate was denoted with a red arrow in the figure, where the origin location was alignment with the center of bearing along the vertical direction, which was consistent with what is described in Fig. 7a.
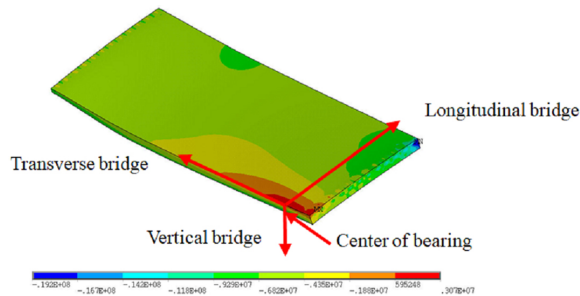

Fig. 9. Longitudinal stress nephogram of the focused concrete deck (Unit: Pa)

As shown in Fig. 9, the tensile stress is large near the origin region. To more clearly show the stress distribution in the concrete deck, the varying curve of stress along the three directions denoted in Fig. 9 using red arrows were extracted and shown in Fig. 10 as follows.

It can be clearly seen that the concrete bridge decks mainly bear compressive stress because the stay cable provides a large compressive stress reserve. However, the local negative moment effect is very significant due to the support of the diaphragm plate. It causes the local tensile stress in the concrete bridge deck, which is 1.92 MPa at the origin position. The local tensile stress decreases quickly along the longitudinal bridge, and becomes compressive stress after 0.43 m away from the origin. There is a longitudinal tensile stress in a specified range along the transverse bridge, and it all becomes compressive
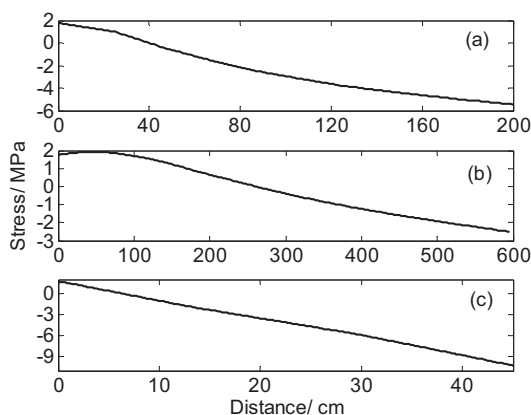
Fig. 10. Varying of longitudinal stress along three directions: (a) longitudinal, (b) transverse, (c) vertical

stress after 2.2 m away from the origin. On the one hand, because the deck is oblique, the top of the deck far from the origin is closer to the neutral axis. On the other hand, the local supporting effect is more prominent near the bearing location. The longitudinal tensile stress varies linearly along the vertical bridge, and it becomes a compressive stress after 0.065 m from the top of the deck.

Comprehensive analysis of the longitudinal stress results of three directions under the completed bridge state, the local stress of the concrete bridge deck is very obvious due to the constraint of bearing and diaphragm plate. There is a tensile stress region of about $0.43 \times 2.2 \times 0.065$ m at the top of the concrete bridge deck, and the maximum tensile stress is 1.92 MPa.

5. Improvement measures

From the above analysis results, we can find a local negative moment and tensile stress region due to the constraints of the bearing and diaphragm plate. To improve the disadvantage force situation of the concrete bridge deck, several improvement measures were proposed, and their efforts were studied as follows.

5.1. The first improvement measure

Because the supporting of the diaphragm induces to large a local negative moment in the concrete bridge deck, here, part of the diaphragm plate connected with the roof at the bearing position was removed. The detailed construction of the improved diaphragm plate was shown in Fig. 11 as follows:
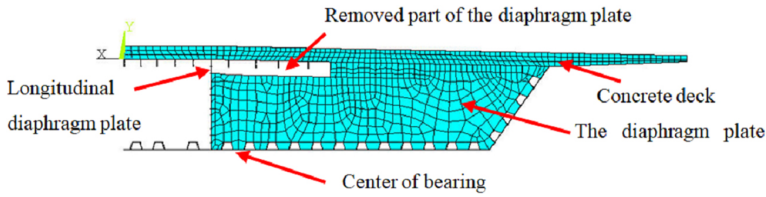
Fig. 11. Detailed construction of the improved diaphragm plate

Through finite element analysis, the stress results of the improved structure were shown in Fig. 12. The varying curve of stress along three directions, which was the same as denoted in Fig. 9, was shown in Fig. 13.
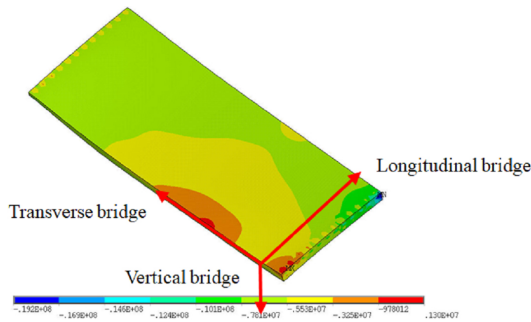

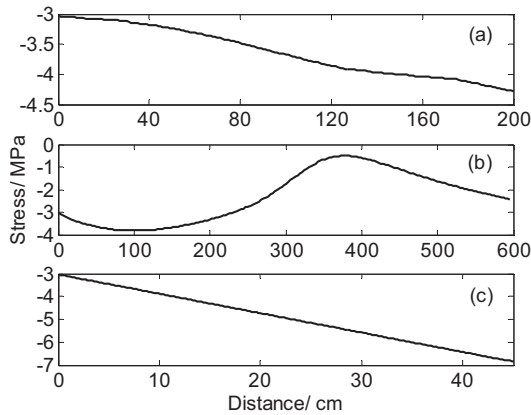Fig. 12. Longitudinal stress nephogram of the concrete deck of the first improved structure (Unit: Pa)

Fig. 13. The varying of the longitudinal stress of the first improved structure along three directions: (a) longitudinal, (b) transverse, (c) vertical

It can be clearly seen that the improved measure dramatically improves the mechanical performance of the concrete deck at the bearing position. After removing part of the diaphragm plate at the bearing position, the local supporting is transferred to the adjacent two

diaphragm plates, which greatly eliminates the peak of negative moment in the concrete deck at the bearing position, and the longitudinal tensile stress is transformed into compressive stress. In addition, the transverse stress is also decreased, so the improvement effort of the first measure is good.

5.2. The second improvement measure

The local strengthening plates were set on the original diaphragm plate at the bearing position, which could enhance the rigidity of the diaphragm plate and bottom plate. However, it only provided limited promotion to the rigidity of roofs. Here, the strengthened plates were extended to two adjacent diaphragm plates, so the supporting effect of the bearing would be dispersed into multi-diaphragm plates, which was beneficial to decrease the local negative moment effect in the concrete bridge deck. The detailed construction of the improved strengthening plate was shown in Fig. 14 as follows:
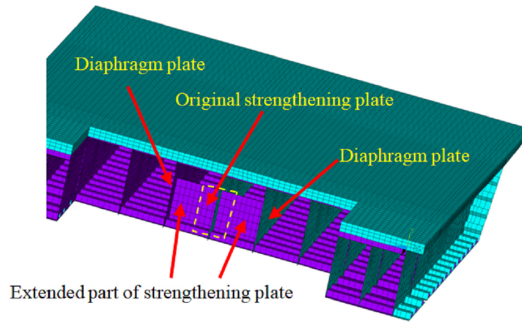

Fig. 14. The detailed construction of the improved strengthening plate

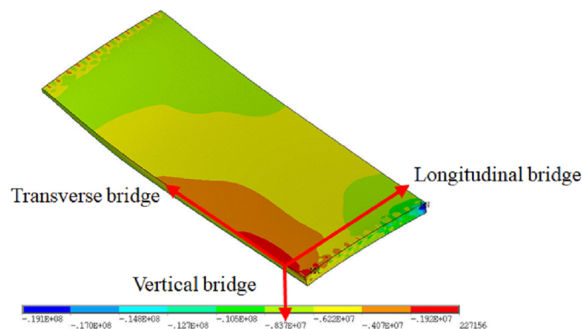The stress results of the improved structure are shown in Figures 15 and 16.

Fig. 15. Longitudinal stress nephogram of the concrete deck of the second improved structure (Unit: Pa)

As shown in the figures, the longitudinal stress in the concrete deck has become the compressive stress after adopting the improvement measure. It is mainly because the extended strengthening plate disperses the supporting of the bearing into three diaphragm
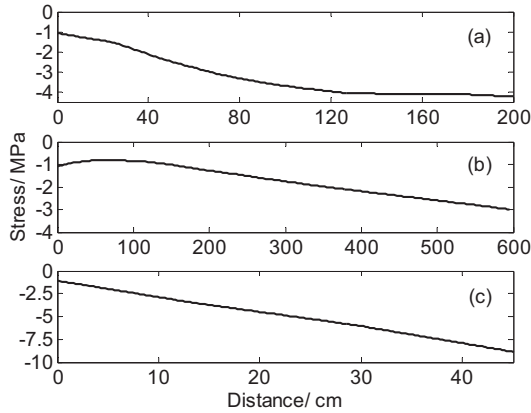
Fig. 16. The varying curve of longitudinal stress of the second improved structure along three
directions: (a) longitudinal, (b) transverse, (c) vertical

plates, which causes more uniform force transmission and peak reduction of the local
negative moment at the bearing position. Therefore, this improvement measure is also very
effective.

5.3. The third improvement measure

The proposed third measure was directly strengthening the local rigidity of the roof by
redesigning the longitudinal ribs under the roof. The original small longitudinal ribs are
24 cm high. Here, we would heighten them to 50 cm and set a steel plate at the bottom
of the longitudinal ribs to connect all ribs. The longitudinal strengthening is limited to
the region between two adjacent diaphragms on both sides of bearing. The detailed structure
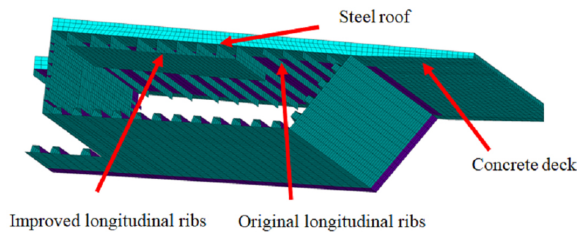of the improved longitudinal ribs was shown in Fig. 17.

Fig. 17. The detailed construction of improved longitudinal ribs

The same finite element analysis and result extracting was carried out, and the analysis
results of the third improvement measure were shown in Fig. 18 and Fig. 19 as follows.

From the above analysis result, we can find that the tensile stress of the concrete deck
reduces to 0.55 MPa, and the range of tensile stress is also shrinking. The tensile stress
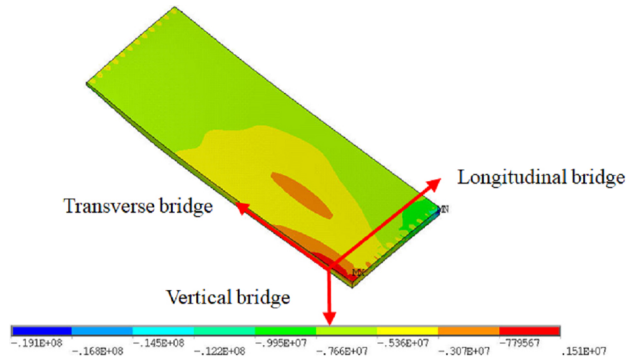
Fig. 18. Longitudinal stress nephogram of the concrete deck of the third improved structure (Unit:Pa)
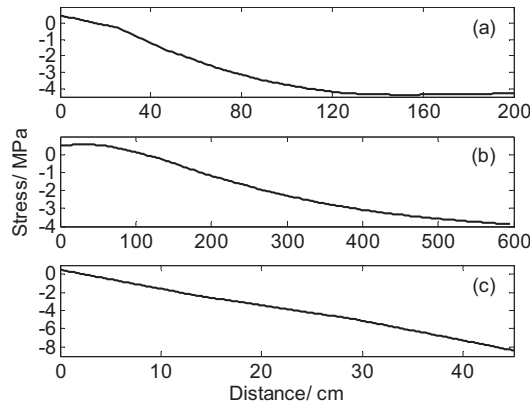

Fig. 19. The varying curve of longitudinal stress of the third improved structure along three directions: (a) longitudinal, (b) transverse, (c) vertical

becomes a compressive stress after 0.19 m away from the origin along the longitudinal bridge. Along the transverse bridge, the concrete deck is all compressive after 0.71 m away from the origin, and it becomes a compressive state after 0.027 m from the top of the deck along the vertical bridge. The improved effect is not better than the above two improvement methods.

5.4. Composed improvement measure

Next, the composed improvement effect when the three measures were adopted simultaneously would be studied. The finite element analysis results of the composed improvement structure were shown in Fig. 20 and Fig. 21.

As shown in the figures, the longitudinal stress in the whole concrete deck has become the compressive stress. The compressive stress increases along the transverse bridge to the cantilever end. It reaches –4.33 MPa at 5.7 m from the center position of the bearing.
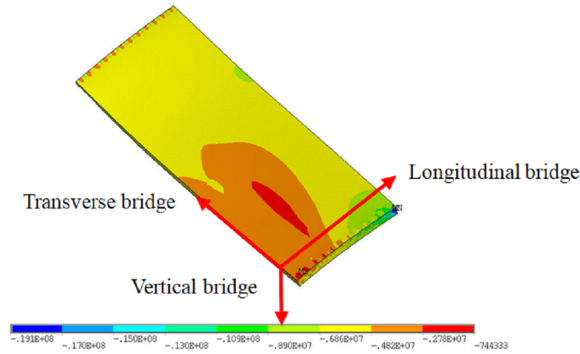
Fig. 20. Longitudinal stress nephogram of the concrete deck of the composed improved structure
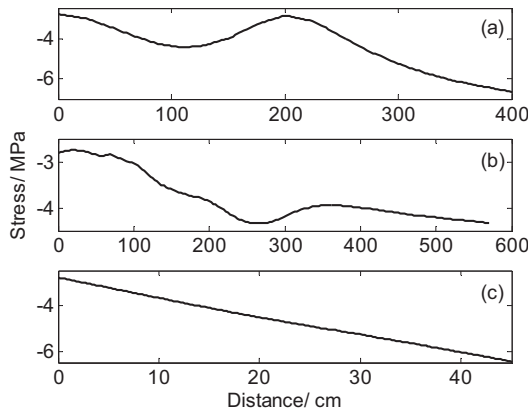(Unit: Pa)

Fig. 21. The varying curve of longitudinal stress of the composed improved structure along three
directions: (a) longitudinal, (b) transverse, (c) vertical

The compressive stress also grows along the vertical from the top of the deck to the bearing
direction, and it reaches –6.46 MPa at the bottom of the concrete deck, which is 0.45 m
down from the top of the deck. The same compressive stress increases to –6.64 MPa along
the longitudinal bridge direction at 4 m from the bearing position. Therefore, the composed
improvement effect of the three measures is prominent.

6. Conclusions

For a semi-floating cable-stayed bridge with a steel-concrete composite girder, the bearing
constraint will induce stress concentration and the peak of negative bending in zero block.
Hence, the concrete bridge deck is at a disadvantage and complex stress state. Aiming at this
problem, the mechanical performance of zero block of a practice semi-floating cable-stayed

has been studied by finite element analysis. Based on the analysis results, three improvement measures have been proposed, and their effects were compared. From the analysis results, we can obtain some conclusions as follows:

1. The numerical analysis results of the full-bridge model show that there is a negative bending moment in the zero block under the complete bridge state. However, the cables provide a large axial pressure on the main beam. Under the combined action of the bending moment and axial force, the whole section of the main beam is in the compressive state, and there is no tensile stress in the upper edge of the concrete deck.

2. Under the support of the diaphragm plate, the local negative moment effect in zero block is very prominent. There is a tensile stress zone of $0.43 \times 2.2 \times 0.065$ m in the concrete bridge deck at the position of the bearing, and the maximum tensile stress is 1.92 MPa.

3. The first improvement measure makes the best effect. By removing part of the diaphragm plate at the bearing position, the local supporting is transferred to the adjacent two diaphragm plates, which can reduce the peak of the negative moment in the concrete deck. The second improvement measure, that is, extending the strengthened plates to two adjacent diaphragm plates, also has a preferable effect. It can disperse the supporting of the bearing into three diaphragm plates, so the force transmission is more uniform. The third measure is directly strengthening the local rigidity of the roof. Compared with the previous two methods, the improved effect of the third measure is slightly weaker.

4. The longitudinal stress in the whole concrete deck has become the compressive stress when the three measures are adopted simultaneously. The composed improvement effect is prominent.

Acknowledgments

References

[1] M. Cai, W. Li, Z. Wan, J. Sheng, J. Tan, and C. Ma, "Cracking control techique for continuous steel-concrete composite girders under negative bending moment", *Archives of Civil Engineering*, vol. 69, no. 3, pp. 239–251, 2023, doi: 10.24425/ace.2023.146078.

[2] Y. Li, T.Guo, L. Bao, and F. Wang, "Determination of force in single cable plane prestressed concrete polygonal line tower cable-stayed bridge based on minimum bending energy", *Archives of Civil Engineering*, vol. 67, no. 3, pp. 565–579, 2021, doi: 10.24425/ace.2021.138071.

[3]   X. Liang, S. Duan, and L. Meng, "Analysis of cross section mechanical properties of steel-concrete composite beam under negative bending moment", *Journal of Shijiazhuang Tiedao University* (*Natural Science Edition*), vol. 33, no. 2, pp. 124–129, 2020.

[4]   V. Jayanthi and C. Umarani, "Performance evaluation of different types of shear connectors in steel-concrete composite construction", *Archives of Civil Engineering*, vol. 64, no. 2, pp. 97–110, 2018, doi: 10.2478/ace-2018-0019.

[5]   B. Grzeszykowski and E. Szmigiera, "Nonlinear longitudinal shear distribution in steel-concret composite beams", *Archives of Civil Engineering*, vol. 65, no. 1, pp. 65–82, 2019, doi: 10.2478/ace-2019-0005.

[6]   Y. Zhao, X. Zhou, Y. Yang, Y.F. Chen, and S. Gurupackiam, "Stiffness and cracking behavior of new U-shaped steel and concrete composite beam under negative bending", *Journal of Structural Engineering ASCE*, vol. 146, no. 5, art. no. 04020046, 2020, doi: 10.1061/(ASCE)ST.1943-541X.0002594.

[7]   B. Liu, Y. Liu, L. Jiang, and K. Wang, "Flexural behavior of concrete-filled rectangular steel tubular composite truss beams in the negative moment region", *Engineering Structures*, vol. 216, art. no. 110738, 2020, doi: 10.1016/j.engstruct.2020.110738.

[8]   A. Song, H. Xu, Q. Luo, and S. Wan, "Finite element analysis on inelastic mechanical behavior of composite beams strengthened with carbon-fiber-reinforced polymer laminates under negative moment", *Frontiers in Materials*, vol. 9, no. 5, art. no. 859663, 2022, doi: 10.3389/fmats.2022.859663.

[9]   Y. Sun, D. Xu, B. Chen, F. Xu, and H. Zhu, "Three-dimensional reinforcement design method and program realization for prestressed concrete box-girder bridges based on a specific spatial lattice grid model", *Engineering Structures*, vol. 175, pp. 822–846, 2018, doi: 10.1016/j.engstruct.2018.08.058.

[10] Y. Sun, S. Dai, D. Xu, H. Zhu, and X. Wang, "New extended grillage methods for the practical and precise modeling of concrete box-girder bridges", *Advances in Structural Engineering*, vol. 23, no. 6, pp. 1179–1194, 2020, doi: 10.1177/1369433219891559.

[11] J. Zhu, X. Wang, and J. Ding, "Experimental study on the flexural behavior of steel-UHPC composite beams with waffle slab in negative moment regions", *China Journal of Highway and Transport*, vol. 34, no. 8, pp. 234–245, 2021.

[12] J. Liu, X. Ma, L. Yan, C. Shen, and X. Zhang, "Research on stress improving method of bridge deck in negative moment zone of steel-concrete composite beam bridge", in *CICTP 2021: Advanced Transportation, Enhanced Connection-Proceedings of the 21st COTA International Conference of Transportation Professionals*. ASCE, 2021, pp. 1293–1301.

[13] H. Kim and C.S. Shim, "Experimental investigation of double composite twin-girder railway bridges", *Journal of Constructional Steel Research*, vol. 65, no. 6, pp. 1355–1365, 2009, doi: 10.1016/j.jcsr.2009.02.004.

[14] C. Xu, Q. Su, C. Wu, and K. Sugiura, "Experimental study on double composite action in the negative flexural region of two-span continuous composite box girder", *Journal of Constructional Steel Research*, vol. 67, no. 10, pp. 1636–1648, 2011, doi: 10.1016/j.jcsr.2011.04.007.

[15] Y. Zhao, X. Zhou, Y. Yang, and S. Gurupackiam, "Stiffness and cracking behavior of new u-shaped steel and concrete composite beam under negative bending", *Journal of Structural Engineering*, vol. 146, no. 5, 2020, doi: 10.1061/(ASCE)ST.1943-541X.0002594.

[16] W. Xue, T. Yang, and L. Bai, "Mechanical behavior of prestressed steel-concrete composite beams under negative moment", *Journal of Wuhan University of Technology*, vol. 34, no. 8, pp. 123–127, 2012, doi: 10.3963/j.issn.1671-4431.2012.08.024.

[17] R. Guo, Q. Su, C. Li, and Q. Deng, "Experimental studies on cracking behavior of post-combined prestressed concrete slab in hogging zone of coposite girder", *Journal of TongJi University* (*Natural Science*), vol. 43, no. 3, pp. 352–356, 2015, doi: 10.11908/j.issn.0253-374x.2015.03.005.

[18] L. Wu and J. Nie, "Analysis of key parameters of non-tensioned prestressing technology for steel-concrete continuous composite beams", *Journal of South China University of Technology* (*Natural Science edition*), vol. 39, no. 4, pp. 156–162, 2011, doi: 10.13206/j.gjgSE19112601.

[19] M. A. Bilal, G. Young, and S. Hamid, "Prestressed composite girders. I: experimental study for negative moment", *Journal of Structural Engineering*, vol. 118, no. 10, pp. 2743–2762, 1992, doi: 10.1061/(ASCE)0733-9445(1992)118:10(2743).

[20] J. Fan, S. Gou, R. Ding, J. Zhang, and Z. Shi, "Experimental and analytical research on the flexural behaviour of steel–ECC composite beams under negative bending moments", *Engineering Structures*, vol. 210, art. no. 110309, 2020, doi: 10.1016/j.engstruct.2020.110309.

[21] X. Shao, Y. Li., Z. Liao, and J. Cao, "Test and finite element analysis on bending performance of UHPC waffle panel", *Journal of China'an Universe: Natural Science Edition*, vol. 38, no. 3, pp. 52–63, 2018.

[22] J. Qi, Y. Bao, J. Wang, L. Li, and W. Li, "Flexural behavior of an innovative dovetail UHPC joint in composite bridges under negative bending moment", *Engineering Structures*, vol. 200, art. no. 109716, 2019, doi: 10.1016/j.engstruct.2019.109716.

[23] H. Qian, Q. Zhang, X. Zhang, E. Deng, and J. Gao, "Experimental investigation on bending behavior of existing RC beam retrofitted with SMA-ECC composites materials", *Materials*, vol. 15, no. 12, pp. 1–19, 2022, doi: 10.3390/ma15010012.